Compressive strength and elasticity of pure lime mortar masonry

Anastasios Drougkas[1], Pere Roca, Climent Molins

Departament d'Enginyeria de la Construcció, Universitat Politècnica de Catalunya, Campus Diagonal Nord, Building C1, Jordi Girona 1-3 UPC, 08034 Barcelona, Spain

Highlights

- The compressive behavior of lime mortar masonry is investigated
- Two types of lime mortars with zero cement content are characterized and applied
- Very high ratio between the compressive strength of the composite and that of mortar is obtained

1. Introduction

The compressive strength of masonry is considered by design codes as the main design parameter, on which, additionally, the derivation of its mechanical properties is largely based. For this reason, masonry in concentric compression has been extensively studied. Taking into account the experimental investigations on masonry composites accompanied by a characterization of the masonry constituents, the instances in the literature become fewer in number. A relatively large number of such experimental investigations has been performed on stack bond prisms [1–14]. Fewer investigations including concentric compression tests on larger members, such as walls in

[1] Corresponding Author
Email addresses: anastasios.drougkas@upc.edu (Anastasios Drougkas), pere.roca.fabregat@upc.edu (Pere Roca), climent.molins@upc.edu (Climent Molins)

running or Flemish bond or three-leaf samples and columns, have been documented in the literature [14–26]. These tests are usually monotonic, but cyclic tests have also been performed [8, 27].

The different combinations of materials present researchers with a wide range of possible choices for experimental study. However, reviewing the available inventory of experimental data, one finds a distinct predominance of cement and lime/cement mortars in structural testing. While chemical, curing, mechanical property and sustainability issues of modern pure lime mortars have been extensively studied [28–34], the investigation of their direct structural application has not enjoyed the same attention [35] despite its common use as original material or for restoration purposes in historical structures.

Measurement of the compressive and flexural strength of units and mortar is well documented and even codified in guidelines [36–38]. However, no comparable effort has been devoted to the characterization of the Young's moduli of the material constituents and the masonry composite. Masonry codes [39] provide empirical relations for the estimation of the masonry Young's modulus using the compressive strength of masonry as the only parameter and hence neglect the important influence of the parameters related to the constituent materials. Regarding experimental procedures, there is a lack of guidelines for the measurement of the Young's modulus of both the units and the mortar as well as of the masonry composite.

Published results on the Young's modulus of units and mortar often do not explain in detail the method used to obtain these results. However, a few studies include a detailed explanation of such measurement methods and often make use of the measured moduli in numerical simulations of the experimental processes [5, 7, 8, 11, 40, 41].

Measurements of the mechanical properties of units are easier to perform and are, therefore, more common. However, compressive tests on the unit beds are usually performed on entire units in the direction perpendicular to the unit bed [4, 5, 21]. Due to the dimensions of units, it is foreseeable that this type of tests is significantly affected by both size and shape effects and hence may not be offering a reliable measurement of the uniaxial compressive strength of the material. By

measuring cylindrical, cubic or cuboid samples extracted from bricks it has been intended to limit or study these size effects or to simply form specimens with appropriate dimensions to facilitate measurements [8, 20, 42].

The issue of the difference between the properties of the mortars in freestanding samples and in the composite persists due to difficulties in obtaining deformation measurements from both the joints, which are prohibitively thin, and from cast samples due to differences in curing conditions. Efforts have been made to measure isolated deformations of the units and the mortar joints in masonry under compression [13, 20]. For other cases, the elastic properties of the mortar in the joints are indirectly derived by measurements in the units and in the composite [25].

The main objective of the experimental campaign herein presented was to determine the compressive strength and Young's modulus of masonry composed of medium strength solid clay bricks and two types of low strength lime/sand mortar with zero Portland cement content. The intention was to establish whether this particular combination of materials can produce composites of adequate compressive strength and, simultaneously, sufficient deformability so as to be, from a structural perspective, compatible with historical masonry for application in intervention projects.

The tests to be performed and the measurements to be taken during their execution were designed so as to give as much information as possible on both the strength and the deformability characteristics of the constituent materials.

2. Description of experimental campaign

The procedures used for the characterization of the component materials and the composite specimens are presented in the following paragraphs.

For the mechanical characterization of the units, it was preferred to measure the uniaxial compressive strength and the Young's modulus of the material of which they are composed, using

appropriate brick cores, rather than measuring the strength of an entire brick in compression. As mentioned above, the latter approach would involve significant size effects in the compression tests. It was also intended to follow a sampling procedure which would allow a large number of testable specimens to be extracted from a single brick. In the case of the application of destructive testing on historical materials this is advantageous for exerting minimum damage and loss of original material in the structure.

The masonry was constructed in stack bond configuration. This geometrical setup allows for a simple way of studying unit-mortar interaction in masonry under concentric compression, as has been noted in integrated experimental/numerical masonry analysis projects [43].

Whenever possible, existing testing standards were consulted in order to compare the parameters in the performed tests and their results against a codified backdrop. It was intended to establish whether the materials and the resulting masonry conform to the application spectrum defined or implied in the corresponding standards.

Units

The units used in the campaign were solid clay bricks with nominal dimensions measuring 290×140×50 mm^3. The bricks were hand-molded, which resulted in the bricks having smaller actual dimensions and rough, uneven surfaces and, often, slanted heads and faces. The more pronounced scatter in the geometric measurements was obtained for the smaller dimensions of the bricks, namely their height.

The bricks received surface treatment prior to testing. The beds were polished in order to ensure smoothness and planarity and to remove surface fissures and other damage, whereupon the bricks were reduced to a height of roughly 40 mm. Following the surface treatment, cylindrical core samples were extracted from the bricks in the direction perpendicular to the unit bed, numbering six to seven from each unit, with a diameter of 45.25 mm. The height to diameter ratio in the samples was, therefore, roughly 1, which is not ideal for eliminating size effects in compression tests or the confinement afforded on the sample by the loading platen, but provides a

significant improvement against the testing of full bricks. Furthermore, the very small height of the bricks, and therefore the very small displacements to be measured, would compound the uncertainty of the measurements. Coring also allows for the influence of local imperfections to be directly measured or even entirely avoided, as internal cracks and voids become visible. Finally, it allows for the clearer overview of the variation of the results, since it may now be decomposed in the variation of the properties between the units as well as in the localized variation of the area from which each sample was extracted. Examples of coring patterns are shown in Figure 1. For these reasons, and in order to obtain some understanding of these size effects, the cylindrical samples were tested in single, double and triple stacks. The surface treatment of the unit beds facilitates this configuration.

The characterization of the tensile strength of the units was done using three-point bending of three complete brick specimens, from which the uniaxial tensile strength may be indirectly determined. There is no EN standard specific to the determination of the tensile or flexural strength of clay units as there are for concrete blocks [36]. Following the aforementioned surface treatment and before testing, the units were placed in a drying oven overnight at a temperature of $105\pm5\ ^{0}C$ to remove existing moisture and to ensure equal moisture for all samples. The units were left to cool for 4 hours prior to testing. The testing was performed using a load cell with a 200 kN capacity in a hinged configuration and displacement measurements were only taken from the load cell readings. The load was applied in force control at a rate of 10 N/sec. The test was performed specifying a central span of 200 mm, as illustrated in Figure 2.

For the compressive tests on the cylindrical samples, a 200 kN capacity load cell was used in a hinged configuration. The load was applied in displacement control, in order to record the softening branch with more ease, at a rate of 0.002 mm/sec. Measurements were taken from three LVDTs placed in the perimeter as shown in Figure 3, and from the load cell readings. These devices were fixed on the loading plates, as the small height of the cylinders, even when stacked, was not sufficient for the LVDTs to be properly attached directly on them. Overall, eleven single samples, eight double samples and six triple samples were tested for a total of 25 compression tests. With the

exception of one triple sample, the doubles and triples were composed of cores from the same brick.

Mortar

Two types of mortar were employed in the construction of the masonry: aerial lime mortar (ALM) and hydraulic lime mortar (HLM) combined with fine sand made of crushed limestone and zero Portland cement content. The ALM mortar was produced in putty form obtained from submersion of CL-90 calcium lime in water in a sealed plastic drum and the HLM directly from NHL 3.5 natural hydraulic lime powder. The properties of the sand are presented in Figure 4 and Table 1. Both mortars were produced in a 1:3 lime-to-sand ratio and were hand-mixed using a trowel. The methodology followed in the characterization of the mortars is described in the EN 1015-11 European standard for mortar testing [37], which includes instructions for the preparation and storing of the samples as well as the testing setups and procedures. However, due to the composition of the mortars, it was immediately understood that this standard is mainly applicable to mortars of higher strength. Nevertheless, it may still be, as it indeed has been, consulted as a guideline for planning this and other similar campaigns.

In parallel with the construction of the prisms, mortar was poured and appropriately compacted in steel 3-compartment molds lubricated with mineral oil to prevent adhesion of the mortar to the mold walls. The mortar was poured in two layers, each of which was compacted with 25 strokes of the tamper. In total, 24 prismatic samples measuring at 160×40×40 mm^3 were prepared for each mortar type. The molds were stored in lab conditions (22.5^0 Celsius, 70.2% humidity) and the samples were extracted after 6 days for the aerial lime and 2 days for the hydraulic lime samples, which were subsequently stored in the same lab conditions. The lack of free contact with the air in the faces of the prisms adjacent to the steel walls of the mold, resulting in very slow hardening, made it necessary to allow a longer period of time to pass before unmolding the aerial lime mortar in order to avoid premature deformation and damage to the samples. Inspection of the molds after removal of the mortar prisms did not reveal any sign of adhered mortar.

The mortars were subjected to flexural and compressive tests. The mortar prismatic samples were tested in three-point bending and the two resulting halves were tested in compression. A 10 kN capacity press was used in force control at a rate of 10 N/s for the bending tests and 50 N/s for the compression tests, both rates corresponding to the minimum standard specified values. The test setups are shown in Figure 5 and the only quantity measured was the force against time. The small dimensions and low strength of the mortars do not allow for accurate displacement measurements to be easily taken. Tests were performed at 14, 28, 42 and 49 days for the ALM and 7, 14, 28 and 49 days for the HLM in order to study the maturation of the mortars.

Masonry

Six masonry wallettes were constructed, three for each mortar type. The EN 1052-1 standard for the determination of the compressive strength of masonry was consulted as a guideline on the preparation of the prisms, the curing and storage, the placement of the measuring instruments and the determination of the loading rate during testing [44]. The masonry wallettes consisted of five bricks and four mortar bed joints of 10 mm thickness, resulting in overall nominal dimensions equaling 290×140×290 mm^3. The bricks were submerged in water for 30 minutes prior to construction, which took place on a flat surface. For each type of mortar, two prisms were capped on both ends using a 3 mm thick sulfur-silica sand mortar joint to ensure the flatness of the loading surfaces, while one prism from each mortar case was capped on the top end with the sulfur-silica sand mortar and a 1.5 mm thick unbonded unreinforced neoprene sheet and with sulfur mortar only on the lower end. Immediately following construction, the prisms were covered with polyethylene sheets for three days in order to prevent premature drying. Subsequently, the masonry was kept in laboratory conditions until it reached an age of 49 days.

The machine used in the compression testing has a static load capacity of 2000 kN. The load cell was set in a hinge configuration to facilitate the adjustment of the load plate with the masonry for uniform load distribution. The load cell was fitted with a short steel profile beam to match the vertical cross section of the prisms. Finally, the masonry was centered between two thick steel plates.

Displacement measurements were taken from 6 LVDTs placed on the masonry, as well as from the readings of the load cell. The LVDTs were placed in such a manner as to measure the vertical deformation of the masonry composite and of an individual unit. The LVDT supports were attached to the masonry using a quick setting adhesive resin. The use of the resin offers good adhesion with minimal disturbance to the surfaces of the units. Placement of the LVDTs often required further surface treatment in the units and the joints in order to properly accommodate their supports and to allow free movement of the instruments. This would not have been necessary in machine-cut bricks.

Due to the irregular heads and faces of the units, the placement of the LVDTs in the exact desired spots was not always possible. For this reason, slight variations of the LVDT setups were attempted, all of which had the same objective. The tests on the aerial lime mortar prisms were performed with a horizontally placed LVDT on the mid height unit to measure the lateral deformation in order to determine the Poisson's ratio. Figure 6 shows such vertical and horizontal LVDT arrangements on the prisms, while Figure 7 presents a schematic view of the two basic LVDT arrangements used.

For the determination of the Young's moduli, and to accommodate the adjustment of the loading platens with the test sample, 5 initial loading cycles under force control were executed with a final cycle maintained at the maximum load for 1 minute before unloading. The initial cycles were performed with a maximum load of 60 kN and the final cycle with a load of 90 kN, all at a load rate of 400 N/s. The cyclic loading process is based on previous suggested procedures for concrete samples [45] and has been applied on masonry prisms as well [8].

Three values of Young's moduli were measured in the masonry: the initial loading modulus measured in the first loading branch during the cyclic tests, the unloading/reloading modulus in the cyclic tests and the final modulus in the monotonic compression test, which was determined at roughly 40-60% of the compressive strength.

The loading to determine the compressive strength was conducted under displacement control in order to capture the post peak response of the masonry. The load was applied at a rate of 0.003 mm/sec. The LVDTs were removed from the structure before the peak in order to avoid damage to the equipment, after which point the only displacement measured was that of the stroke of the actuator. Therefore, information for the Young's modulus could be obtained from this set of tests as well. The test was stopped once the post peak curve reached roughly 5-10% of the obtained capacity.

Direct measurement of the Young's modulus of the mortars was impractical both on freestanding samples as on the masonry itself. Test samples were required to be of small size, otherwise mortar hardening would not be achieved within a practical time limit, and therefore direct placement of measuring equipment was not possible. As an alternative course of action, the Young's modulus of the mortars may be indirectly determined. This can be achieved following the measurement of the Young's modulus of the units and of the masonry composite by a simple, one-dimensional homogenization process. This process idealizes the masonry composite as a set of linear elastic springs in series. According to this, the elastic modulus of the masonry composite E_c is calculated by the following equation:

$$E_c = \frac{1 + h_m / h_u}{1 + h_m \cdot E_u / \left(h_u \cdot E_m \right)} E_u \tag{1}$$

where h_m and h_u are the thickness of the mortar bed joint and the height of the units respectively and E_m and E_u are the Young's moduli of the mortar and the units. The model assumes perfect normal and shear bond in the unit-mortar interface as well as neglecting Poisson effects, which do not have a strong influence on vertical masonry stiffness for stack bond prisms.

3. Results

Units

The results of the bending tests on the bricks are presented in Table 2. Despite the small number of tests, the results were consistent and showed very little scatter. The tensile strength of the brick f_{tu} is derived from the flexural strength f_{flex} by way of equation (2), where *h* is the specimen height [46].

$$f_t = \frac{0.06 \cdot h^{0.7}}{1 + 0.06 \cdot h^{0.7}} f_{flex} \quad (2)$$

The compressive test results on the core samples are presented in two tables. The results and dimensions of the samples, organized according to the number of cylinders in the sample, are presented in Table 3. Similarly, Table 4 summarizes the same results according to the brick from which the samples were extracted regardless of sample size. This distinction allows to overview the variation of the results according to the parent brick and the sample size. The bricks are again designated by roman numerals (it is reminded that I, II and III where the ones tested in bending) and the extracted samples by ordinary numerals.

The failure mode of the samples may be seen in Figure 8. Vertical and diagonal cracks in the stacked specimens jump across the polished interfaces, indicating good contact between the samples. Continuity of spalling damage was also noticed.

It was noticed that imperfections such as existing cracks did not have a strong influence on the compressive strength or stiffness of the samples, as compared to undamaged samples from the same brick. However, damage at the base or the top of the samples, mostly due to the coring process, caused a notable reduction of the strength of the samples.

Examining the results of each brick separately, for example bricks II, III and IV, the compressive strength showed a decreasing trend for an increase in sample height. On the contrary, the Young's modulus increased with the specimen height throughout all the cases and on a brick by brick basis, despite the fact that the increase of the height of the specimens, which reduces size effects, and the existence of horizontal joints normally result in a decrease of the axial stiffness. Of further note is the fact that the scatter of the results for the Young's modulus exhibited a marked

decrease for an increase in height, even though the number of tests was smaller for larger heights. The scatter of the results on the compressive strength was also the lowest across the triple sample cases.

Moderate variation was discovered in the properties across the bricks, with units VI and VII having a Young's modulus significantly higher than the average and unit I having a compressive strength higher than the average. These trends appear to have been partly influenced by the properties of the individual bricks from which the samples were extracted. For example, half of the triple stacked samples were performed using cores from units VI and VII, which had the highest Young's modulus. Finally, there was no correlation between the flexural strength of the brick and the compressive strength of the samples extracted from it.

Mortars

The evolution of the strength of the two mortars presents a number of differences. This can be attributed to the different maturation process between the binding agents in the two materials considered, aerial and hydraulic lime. Figure 9 illustrates the evolution of the compressive and flexural strength of the two mortars [47].

The compressive strength of the ALM exhibited a low initial rate of increase, which tended to decrease after 28 days. At 49 days the rate of increase was low but not zero. The HLM exhibited significant strength at 7 days, compared to the one achieved at 49 days. However, the rate of increase of strength was comparatively low in the remaining period until 49 days. The difference in both cases between the values at 28 and 49 days is significant, however, and should be considered in structural design.

It is unclear whether further maturation of the mortar would result in even higher compressive strength values or how long it would take for a substantial increase. Evaluation of the tendency lines for the compressive strength seems to indicate that near maximum strength could be reached at 49 days for the HLM, but ALM should be expected to increase further in strength, as is evidenced by practical experience and the obtained development curve. Due to the scatter obtained

for the flexural strength of the ALM it is difficult to make a similar estimation, though much higher strength should not be expected. However, the flexural strength of the HLM appears to be increasing significantly even after the 49th day.

The results of the mortar bending tests at 49 days are presented in detail in Table 5, where the dispersion of results in the case of the ALM is apparent, whereas the dispersion in the case of the HLM was much smaller. Taking into consideration that the tensile strength of the mortar is not significant in the study of the compressive strength of masonry, especially in stack bond prisms, the scatter of the aerial lime results is of small consequence. Despite using the lowest value of load application rate specified in the standard, failure was reached at a time as short as 10 sec, which is lower than 30 sec specified in the standard as the shortest recommended duration of the test.

The results obtained from the compressive tests at 49 days for both mortar types are presented in detail in Table 6. The samples are named after the mortar prisms tested in bending from which they were produced with the added suffix a or b. Once again, only the actuator force in time was measured. As was the case with the unit tests, no distinct relation between flexural and compressive strength of samples from the same prism could be discerned. Overall, the scatter of the results was quite low and much lower than for the bending tests.

According to the EN standard, mortar bending and compressive tests should be performed at an age of 28 days unless retarding agents have been employed in the mix, which was not the case in this campaign. Overviewing the results, it is apparent that the increase in strength in the period between 28 and 49 days is significant compared to, for example, the corresponding increase for concrete or masonry mortars based on Portland cement stored in laboratory conditions.

Masonry

The cyclic loading of the prisms initially performed for each specimen revealed certain aspects of the masonry's response. The initial response in compression is highly nonlinear, as micro-cracks in the unit-mortar interface and voids in the mortar are closed. Unloading, even when only a very small load has been applied, has a far higher elastic modulus than the initial one in compression.

The compressive loading modulus eventually becomes equal to the unloading one, provided sufficient load has been applied. This behavior is illustrated in Figure 10. Considering this fact, it may be necessary to perform these loading cycles using a higher load in order to get readings of the Young's modulus after the closing of the voids. However, special care must be taken in the case of weak component materials in order to limit the risk of premature damage in the masonry specimen.

Significant agreement was found between the values of the capacity obtained for the two prisms with the sulfur mortar cap (prisms 1 and 3). The stress-displacement diagrams for the ALM masonry prisms are shown in Figure 11 and the results are summarized in Table 7. The failure mode was similar as well. The first visible cracks were observed at around 70% of the load and they included diagonal cracks originating from near the edges of the top of the prism and were mostly visible on the faces of the units. As cracking progressed, peripheral superficial cracking developed which eventually outlined a mostly crack-free core of masonry with its minimum width at mid height and spreading to the top and bottom units, which were almost intact. The condition of the ALM masonry at the end of the test is shown in Figure 12.

The prism with the neoprene sheet as the top compensating layer exhibited a lower strength value and a different failure mode. Whereas the sulfur mortar layer provides a certain degree of confinement on the top and bottom units, as is demonstrated by the largely undamaged state they are in at the end of the test, the neoprene layer affords the opposite effect. The lateral expansion of the sheet causes major vertical cracks at mid length of all the faces of the top unit for a very low load. Further load increase leads to the formation of new vertical cracks, in parallel with the first central crack, as well as to the perimetrical spalling noticed in the sulfur cap cases. At the end of the test the top unit was found to be significantly cracked, while the bottom unit was once again free from extensive damage.

At the end of the test, the remaining cores were inspected and manipulated and were found to be very fragile, which is to be expected from the fact that the test was continued until a very low level of residual strength. The sulfur mortar caps were also inspected, and, apart from limited

damage near the edges of the masonry where the perimetrical spalling had affected the top and bottom units, they were found to be intact. The neoprene sheet did not show significant damage.

In all three cases the mortar was found to be in a much deteriorated state due to crushing. The smooth post peak curve appears to indicate that the failure is governed by compressive yielding, which would account for the amount of energy release. Furthermore, examination of the samples after testing revealed that the mortar had no residual strength and even completely lacked integrity, especially near the edges of the masonry. Finally, the detached pieces of brick had hardly any mortar adhering to the beds, indicating either a poor tensile and shear bond or simply complete deterioration of the mortar due to crushing.

It is possible that the carbonation of the mortar near the center of the joints was incomplete due to lack of free contact with the air. In this case, complete carbonation of the entire mass of mortar would require a significant amount of time. This could account for the fragility and instability of the remaining masonry core.

The initial and unloading/reloading Young's moduli of the ALM masonry measured from the cyclic tests were lower and higher respectively than the final value registered in the monotonic compression test. The average ratio of the final Young's modulus in the monotonic test over the compressive strength was 53.2.

The HLM prisms exhibited higher capacity and global stiffness and an apparent shift in failure mode. Although the initiation and propagation of cracking was similar to the ALM case, as was the fact that the top and bottom units remained mostly undamaged, there were a number of noticeable differences. Firstly, the mortar retained its integrity to a higher degree, as was evident by inspection of the mortar masses adhering to the broken off pieces of brick as well as the existence of intact mortar pieces which, after manual manipulation, did not exhibit signs of significant crushing. Furthermore, the mortar in the remaining core was not crushed. Hydraulic lime should not normally experience problems with curing in areas not in free contact with air.

There appeared to be evidence of more extensive unit cracking than in the ALM case. The broken off pieces of brick were generally of smaller size and there was noticeable presence of unit dust, which was not present in the ALM samples. Due to the relatively high compressive strength of the units, it seems unlikely that the unit dust is the result of unit crushing. Overall, the above evidence appears to point towards a more prevalent influence of unit cracking in the failure mode. The condition of the HLM masonry after the test is shown in Figure 13,

The HLM post peak curves were also of a different overall shape, featuring steep, almost vertical, decline in the resisting force. However, the remaining masonry core was more stable than in the ALM cases and mostly intact due to the better condition the mortar was in at the end of the test. The steeper post peak curves corroborate the point of higher involvement of cracking in the failure.

The HLM prism with the neoprene cap (prism 3) exhibited a lower compressive strength than the corresponding ALM prism. The failure mode was again similar across both material types, with extensive cracking at the top unit in the HLM case. The neoprene sheet itself was torn at the end of the test, but it could not be determined whether the failure of the sheet was responsible for the reduced apparent capacity of the masonry. The load displacement graphs for the HLM masonry are shown in Figure 14.

Both the values of the initial and unloading reloading Young's moduli measured in the cyclic tests were higher than the value recorded during the monotonic compression tests. The average ratio of the final Young's modulus over the compressive strength was 89.81.

The vertical deformation measurements, obtained by means of the LVDTs placed in this direction, are presented in Table 7 and Table 8. The mean value for the Young's modulus of the units measured directly in the masonry considering all six cases was 6031 MPa, but the coefficient of variation was 1.06. The results from the compressive strength tests on the units should, for all intents and purposes, be considered more reliable for determining the Young's modulus of the

units. However, it is worth noting that the brick Young's modulus measured in the masonry agrees with the one measured in the compressive tests carried out on three stacked samples.

Having acquired the values of the Young's modulus for the units and the two masonry composites it is possible, through equation (1), to estimate the Young's modulus of the mortars. The resulting Young's moduli for the ALM and HLM are

$$E_{m,aerial} = 125MPa$$

$$E_{m,hydraulic} = 250MPa$$

The horizontal measurements in the central brick were also successful. The average Poisson's ratio v_u over the three ALM cases was 0.162. These results could not be based on the cyclic tests but on the monotonic tests for the determination of the masonry strength, as the horizontal deformation in the former proved to be too low to be measured accurately.

The development of the cracks typically observed in the masonry is illustrated in Figure 15, where the location and order of appearance of visible crack damage is shown for the two capping methods used. Similar crack development was noted for both ALM and HLM masonry.

For both mortar types, the units and both masonry composites, the ratio between the Young's modulus and the compressive strength was significantly lower than the ratios reported in the literature and particularly lower than the ratios provided as rough estimations in design codes, such as Eurocode 6 [39].

Another major discrepancy between these experimental results and standard design code provisions is in the prediction of the compressive strength of the masonry from that of the two component materials. The Eurocode 6 equation for the characteristic compressive strength of standard masonry composed of clay units and general purpose mortar, such as the ones used in this campaign, reads:

$$f_c = 0.5 f_{c,u}^{0.7} f_{c,m}^{0.3} \quad (3)$$

Equation (3) results in a value of 4.7 MPa for the aerial lime mortar masonry and 5.4 MPa for the hydraulic lime masonry, which are much lower than the experimentally derived values.

In the present experiments, an increase of 50% in the compressive strength of mortar, that being the difference between the two mortars tested, only resulted in a 14% increase in the compressive strength of the masonry composite, considering only the sulfur cap cases. This result is almost entirely consistent with the exponent on the mortar compressive strength which yields an increase of 13% for the composite when the mortar strength increases by 50%. In terms of compressive strength alone, the composite specimens were, in contrast with the mortars, more within the applicability spectrum implied in the EN 1052-1 standard for masonry compression testing.

Throughout all the cases the failure mode remained consistent. It was mostly influenced by the capping method, as was the compressive strength. The two capping materials did not have a significant effect on the global stiffness of the test setup, due to their very low thickness, with slightly lower global stiffness in the neoprene cases, as measured in the readings of the stroke of the actuator. The LVDT readings are, however, independent of the capping, since they were anchored on the masonry and not on the loading plates. The deformation of the composite specimen accounted for almost the entire deformation of the setup as noted by comparing the stiffness according to the actuator displacement and the deformation of the samples only.

Concerning the measurement instruments used, the removal of the LVDTs prior to the stress peak may not have been entirely necessary, given the fact that the load is applied in displacement control, thus eliminating the possibility of explosive failure and, therefore, of damage to the instruments. Near the peak the vertical deformation is more uniform, which would allow for better measurements to be obtained.

4. Conclusions

In the present work, a series of masonry materials frequently present in historical structures, namely fired clay bricks, aerial calcium mortar and hydraulic calcium mortar, was characterized mechanically. These materials were used in the construction of masonry prisms, which were subsequently tested in compression. A number of conclusions were drawn from these experiments.

Firstly, it has been established that relatively high masonry strength can be consistently achieved using conventional lime mortars and moderately strong units. Specifically, it was possible to achieve masonry strength nearly 10 times higher than the compressive strength of the mortar. Additionally, it was observed that a significant amount of energy absorption is possible, especially in failure modes dominated by mortar crushing. In order to achieve this high masonry compressive strength the samples were tested at 49 days instead of the standard 28, a significant increase in the compressive strength of the mortar being registered in the intervening time.

The lime mortars tested in this campaign appear to be situated slightly below the spectrum of mortars covered by the EN 1015-11 standard. This was made apparent due to their low resulting strength, the length of time required for maturity and the very low loading rates necessary for adequately controlled and, therefore, accurate testing, which, nevertheless, resulted in the maximum load to be reached before the time specified by the standards.

The resulting masonry composites had a compressive strength much higher than the ones predicted by the EN standard. However, the relative increase in the compressive strength of masonry for an increase in the compressive strength of the mortar was consistent with the increase predicted by the EN standard, even though the prediction was incorrect in terms of absolute values.

Lime mortar specimens present a number of difficulties during experimental testing due to their low strength and curing characteristics. Due to their low strength, it may be inappropriate to use modern testing standards for their characterization. Moreover, and due to the slow curing process experienced by them, only small specimens can be reliably tested, especially for aerial lime mortars. As far as the testing and measuring equipment is concerned, larger specimens, such as

cylinders, might provide more accurate measurements of the mechanical properties; however, the proper curing throughout the specimen would not be achieved before a very long time.

Employing the coring method for extracting samples from the units, it was possible to obtain sufficient specimens for one bending test and between two and six compressive strength/Young's modulus tests, depending on the number of cores in the compressed stack. Given sufficient brick dimensions, several tests may be performed on a single brick, making the method an interesting choice for historical brick testing.

Boundary conditions during masonry testing, as influenced by the capping method, can have a pronounced effect on the estimation of masonry strength and the obtained failure mode. Sulfur caps provide lateral confinement to the masonry and limit the initiation of failure in the mid-height of the masonry. On the other hand, neoprene caps caused premature failure near the load platen due to excessive lateral expansion of the neoprene sheet.

Acknowledgments

The present study has been supported by funding procured through the SUBTIS project (Study of the Sensitivity of Urban Buildings to Tunneling Induced Settlements, BIA2009-13233) funded by *Ministerio de Educación y Ciencia* and the ERDF (*European Regional Development Fund*).

References

1. Barbosa CS, Lourenço PB, Hanai JB (2010) On the compressive strength prediction for concrete masonry prisms. Mater Struct 43:331–344. doi: 10.1617/s11527-009-9492-0

2. Furtmüller T, Adam C (2011) Numerical modeling of the in-plane behavior of historical brick masonry walls. Acta Mech 221:65–77. doi: 10.1007/s00707-011-0493-z

3. Hamid AA, Chukwunenye AO (1986) Compression behavior of concrete masonry prisms. J Struct Eng 112:605–613.

4. Kaushik HB, Rai DC, Jain SK (2007) Stress-Strain Characteristics of Clay Brick Masonry under Uniaxial Compression. J Mater Civ Eng 728–739.

5. McNary WS, Abrams DP (1985) Mechanics of Masonry in Compression. J Struct Eng 111:857–870.

6. Hossain MM, Ali SS, Azadur Rahman M (1997) Properties of Masonry Constituents. J Civ Eng Inst Eng Bangladesh CE 28:135–155.

7. Mohamad G, Lourenço PB, Roman HR (2007) Mechanics of hollow concrete block masonry prisms under compression: Review and prospects. Cem Concr Compos 29:181–192. doi: 10.1016/j.cemconcomp.2006.11.003

8. Oliveira DV de C, Lourenço PB, Roca P (2006) Cyclic behaviour of stone and brick masonry under uniaxial compressive loading. Mater Struct 39:247–257. doi: 10.1617/s11527-005-9050-3

9. Panizza M, Garbin E, Valluzzi MR, Modena C (2012) Experimental investigation on bond of FRP/SRP applied to masonry prisms. 6th Int. Conf. FRP Compos. Civ. Eng. 2012. pp 13–15

10. Sarangapani G, Reddy BVV, Jagadish KS (2005) Brick-Mortar Bond and Masonry Compressive Strength. J Mater Civ Eng 229–237.

11. Vyas CVU, Reddy BVV (2010) Prediction of solid block masonry prism compressive strength using FE model. Mater Struct 43:719–735. doi: 10.1617/s11527-009-9524-9

12. Reddy BVV, Lal R, Nanjunda Rao KS (2009) Influence of Joint Thickness and Mortar-Block Elastic Properties on the Strength and Stresses Developed in Soil-Cement Block Masonry. J Mater Civ Eng 21:535–542.

13. Vermeltfoort AT, Martens DRW, van Zijl GPAG (2007) Brick–mortar interface effects on masonry under compression. Can J Civ Eng 34:1475–1485. doi: 10.1139/L07-067

14. Gumaste KS, Nanjunda Rao KS, Reddy BVV, Jagadish KS (2007) Strength and elasticity of brick masonry prisms and wallettes under compression. Mater Struct 40:241–253. doi: 10.1617/s11527-006-9141-9

15. Almeida C, Guedes JP, Arêde a., et al. (2012) Physical characterization and compression tests of one leaf stone masonry walls. Constr Build Mater 30:188–197. doi: 10.1016/j.conbuildmat.2011.11.043

16. Aprile A, Benedetti A, Grassucci F (2001) Assessment of cracking and collapse for old brick masonry columns. J Struct Eng 127:1427–1435.

17. Binda L, Fontana A, G. Frigerio (1988) Mechanical behaviour of brick masonries derived from unit and mortar characteristics. 8th Int. Brick Block Mason. Conf. Vol.1, Dublin, Irel. pp 205–216

18. Binda L, Pina-Henriques JL, Anzani A, et al. (2006) A contribution for the understanding of load-transfer mechanisms in multi-leaf masonry walls: Testing and modelling. Eng Struct 28:1132–1148.

19. Brencich A, Sterpi E (2006) Compressive Strength of Solid Clay Brick Masonry: Calibration of Experimental Tests and Theoretical Issues. Struct. Anal. Hist. Constr. New Delhi 2006. pp 757–766

20. Domède N, Pons G, Sellier A, Fritih Y (2009) Mechanical behaviour of ancient masonry. Mater Struct 42:123–133. doi: 10.1617/s11527-008-9372-z

21. Eslami A, Ronagh HR, Mahini SS, Morshed R (2012) Experimental investigation and nonlinear FE analysis of historical masonry buildings – A case study. Constr Build Mater 35:251–260. doi: 10.1016/j.conbuildmat.2012.04.002

22. Ewing BD, Kowalsky MJ (2004) Compressive Behavior of Unconfined and Confined Clay Brick Masonry. J Struct Eng 130:650–661.

23. García D, San-José JT, Garmendia L, San-Mateos R (2012) Experimental study of traditional stone masonry under compressive load and comparison of results with design codes. Mater Struct 45:995–1006. doi: 10.1617/s11527-011-9812-z

24. Milosevic J, Gago A, Lopes M, Bento R (2012) Experimental Tests on Rubble Masonry Specimens–Diagonal Compression, Triplet and Compression Tests. 15th World Conf. Earthq. Eng.

25. Page AW (1981) The biaxial compressive strength of masonry. Proc. Inst. Civ. Eng. pp 893 – 906

26. Riddington JR, Naom NF (1994) Finite element prediction of masonry compressive strength. Comput Struct 52:113–119.

27. Naraine K, Sinha S (1991) Cyclic behavior of brick masonry under biaxial compression. J Struct Eng 117:1336–1355.

28. Binda L, Papayianni I, Toumbakari E, Hees R van (2002) Mechanical tests on mortars and assemblages. Characterisation Old Mortars with Respect to their Repair - Final Rep. RILEM TC 167-COM. pp 57–76

29. Callebaut K, Elsen J, Balen K Van, Viaene W (2001) Nineteenth century hydraulic restoration mortars in the Saint Michael's Church (Leuven, Belgium): Natural hydraulic lime or cement? Cem Concr Res 31:397–403.

30. Degryse P, Elsen J, Waelkens M (2002) Study of ancient mortars from Sagalassos (Turkey) in view of their conservation. Cem Concr Res 32:1457–1463.

31. Drdácký M, Masin D, Mekonone MD, Slizkova Z (2008) Compression tests on non-standard historic mortar specimens. 1st Hist. Mortar Conf. 24-26 Sept. 2008, Lisbon. pp 24–26

32. Lanas J, Alvarez-Galindo JI (2003) Masonry repair lime-based mortars: factors affecting the mechanical behavior. Cem Concr Res 33:1867–1876. doi: 10.1016/S0008-8846(03)00210-2

33. Lanas J, Pérez Bernal JL, Bello M a., Alvarez-Galindo JI (2004) Mechanical properties of natural hydraulic lime-based mortars. Cem Concr Res 34:2191–2201. doi: 10.1016/j.cemconres.2004.02.005

34. Lanas J, Pérez Bernal JL, Bello M a., Alvarez-Galindo JI (2006) Mechanical properties of masonry repair dolomitic lime-based mortars. Cem Concr Res 36:951–960. doi: 10.1016/j.cemconres.2005.10.004

35. Costigan A, Pavía S (2012) Influence of the mechanical properties of lime mortar on the strength of brick masonry. 2nd Conf. Hist. Mortars. pp 349–360

36. CEN (2005) EN 1996-1-1: Rules for reinforced and unreinforced masonry.

37. CEN (2002) UNE-EN 772-6 - Métodos de ensayo de piezas para fábrica de albañilería - Parte 6: Determinación de la resistencia a flexotracción de las piezas de hormigón de árido para fábrica de albañileria.

38. CEN (2011) EN 772-1 - Métodos de ensayo de piezzas para fábrica de albañilería - Parte 2: Determinción de la resistencia a compresión.

39. CEN (2007) EN 1015-11 - Methods of test for mortar for masonry - Part 11: Determination of flexural and compressive strength of hardened mortar.

40. (1997) Structural Masonry: An Experimental/ Numerical Basis for Practical Design Rules (CUR Report 171). Taylor & Francis

41. Vermeltfoort AT, Pluijm R (1999) Materiaalparameters voor constructief metselwerk. Report 193, CUR, Gouda, The Netherlands

42. Atkinson R, Amadei B, Saeb S, Sture S (1989) Response of masonry bed joints in direct shear. J Struct Eng 115:2276–2296.

43. Rots JG (1994) Structural masonry: An experimental/numerical basis for practical design rules. Report 171, CUR, Gouda, The Netherlands

44. CEN (1999) EN 1052-1 - Methods of test for masonry - Part 1: Determination of compressive strength.

45. Associação Brasileira de Normas Técnicas (2004) NBR 8522 - Concreto - Determinação dos módulos estáticos de elasticidade e de deformação e da curva tensão- deformação.

46. CEB-FIP (2012) Model Code 2010 Volume 1.

47. Tohidi M (2012) Experimental Mechanical Characterization of Historical Mortars by Windsor Pin Penetrometer. MSc dissertation, Department of Strength of Materials and Structural Engineering, Technical University of Catalonia, Barcelona Spain

Notation

E_u	Young's modulus of units
E_m	Young's modulus of mortar
E_c	Young's modulus of masonry
f_{cu}	Uniaxial compressive strength of units
f_{cm}	Uniaxial compressive strength of mortar

$f_{c,exp}$	Experimentally derived compressive strength of masonry
$f_{flex,u}$	Flexural strength of units
f_{tu}	Tensile strength of units
$f_{flex,m}$	Flexural strength of mortar
v_u	Poisson's ratio of units
h_u	Height of units
l_u	Length of units
t_u	Width of units
h_m	Thickness of mortar bed joint

Figure Captions

Figure 1 Sample extraction pattern: full bricks and half bricks obtained from bending test.

Figure 2 Brick flexural strength setup.

Figure 3 Test and measurement layout for compressive tests: (a) single, (b) double and (c) triple samples.

Figure 4 Sand grain size cumulative curve.

Figure 5 Mortar testing setup: (a) bending before and (b) after test, and (b) compression test before and (d) after test.

Figure 6 Typical layout of LVDTs: (a) vertical layout for displacement measurement in the unit and the composite and (b) horizontal displacement for measurement of the Poisson's ratio.

Figure 7 Schematic of two LVDT placement arrangements: (a) vertical measurements only (HLM) and (b) vertical and horizontal deformation measurement (ALM).

Figure 8 Samples after testing. (a) single, (b) double and (c) triple samples. Continuity of the vertical cracks is visible in the stacked samples.

Figure 9 Evolution of mortar compressive (left) and flexural strength (right).

Figure 10 Cyclical loading response of prisms.

Figure 11 Stress displacement diagrams for aerial lime prisms. Neoprene sheet used for prism 2.

Figure 12 ALM prisms after testing: (a) with sulfur mortar cap and (b) with neoprene sheet.

Figure 13 HLM prisms after testing: (a) with sulfur mortar cap and (b) with neoprene sheet.

Figure 14 Stress displacement diagrams for hydraulic lime prisms. Neoprene sheet was used for prism 3.

Figure 15 Crack development in masonry: front and side view of prisms (a) with sulfur mortar caps and (b) with neoprene top cap, the numbers indicating order of appearance.

Table Captions

Table 1 Sand properties

Table 2 Unit three-point bending test results.

Table 3 Unit core compression results sorted according to sample size.

Table 4 Unit core compression results sorted according to sampled brick.

Table 5 Mortar flexural strength results.

Table 6 Mortar compressive strength results.

Table 7 Masonry compressive strength results for ALM prisms. Neoprene sheet was used for prism 2.

Table 8 Masonry compressive strength for HLM prisms. Neoprene sheet was used for prism 3.

colour figure

Click here to download high resolution image

colour figure

Click here to download high resolution image

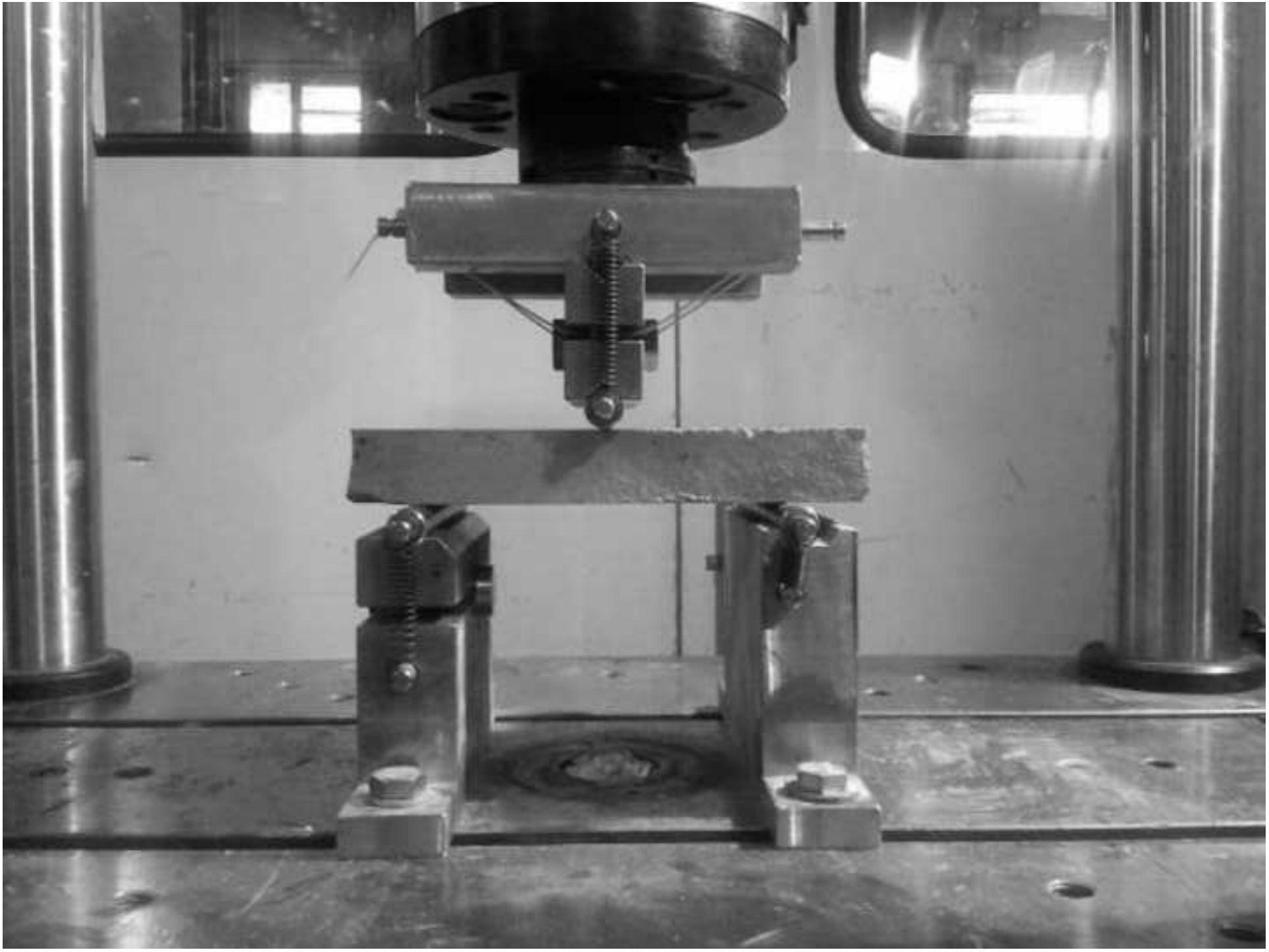

line figure
Click here to download line figure: fig3.eps

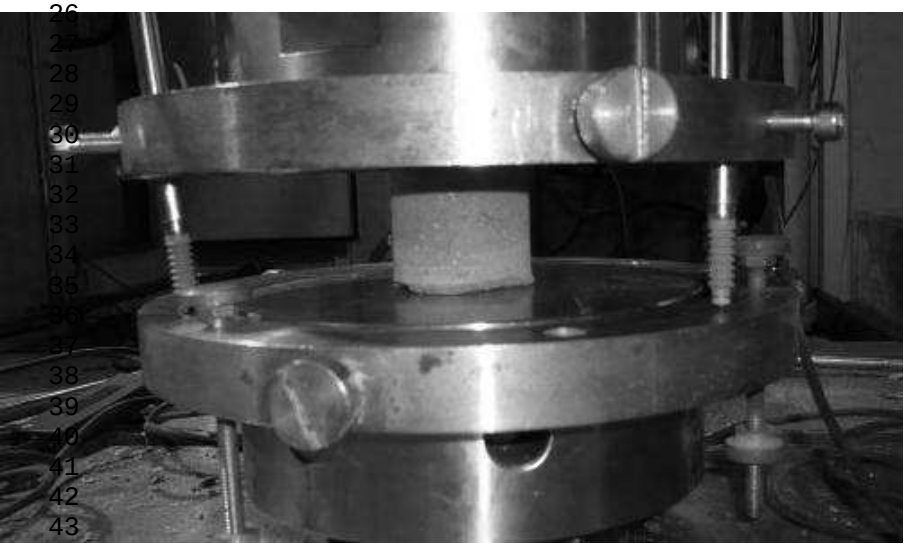

(a)

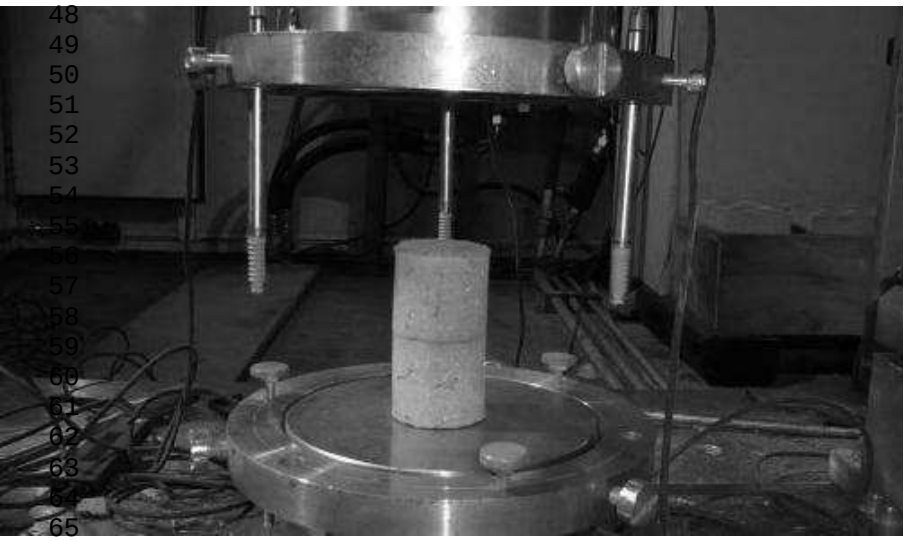

(b)

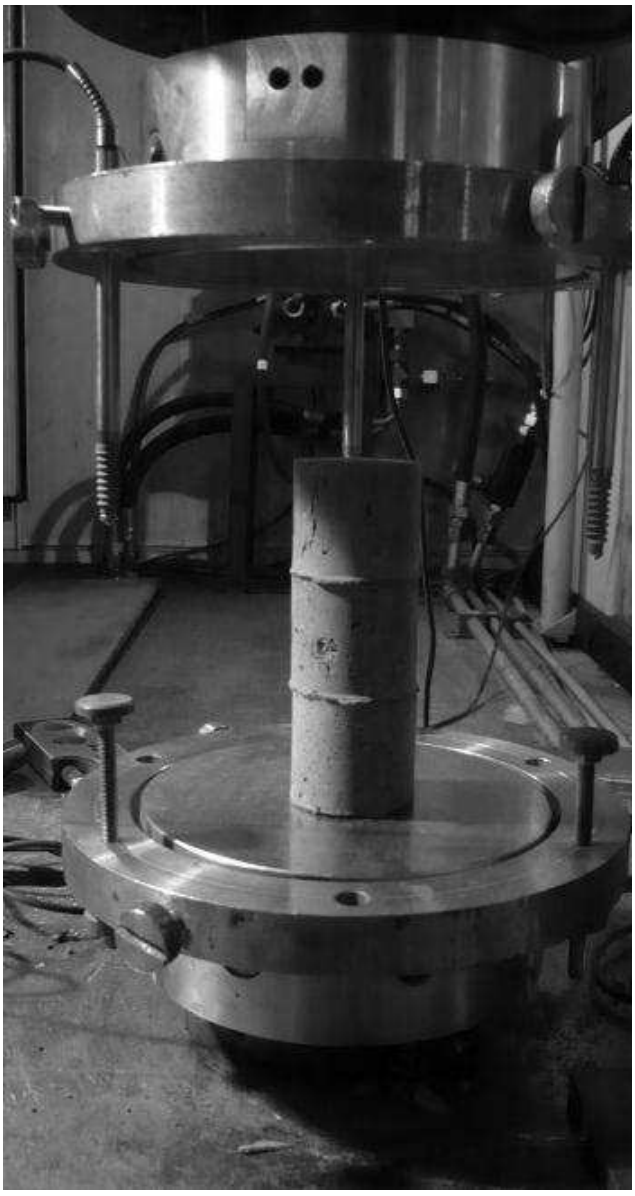

(c)

line figure

Click here to download line figure: fig4.eps

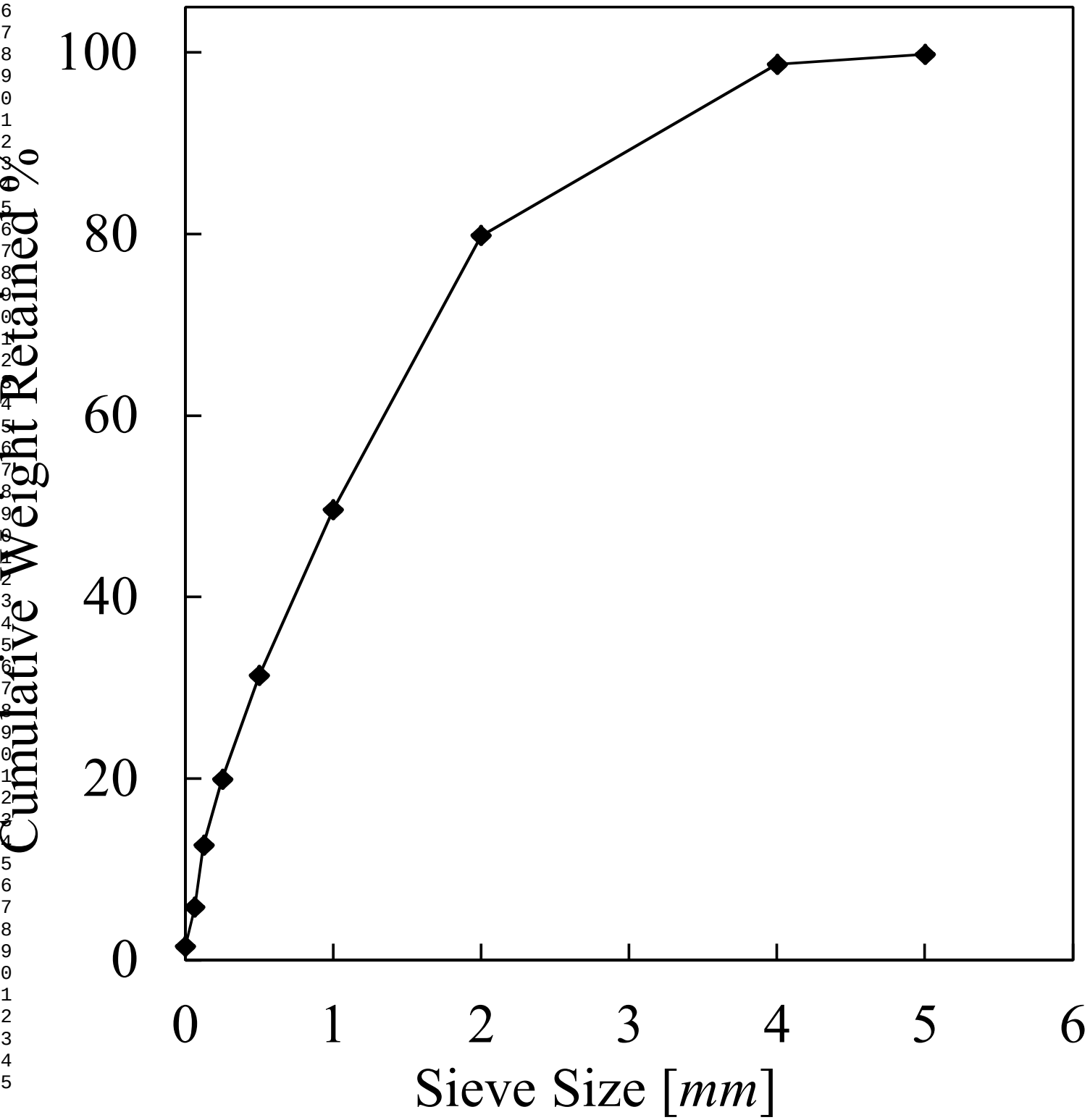

line figure
Click here to download line figure: fig5.eps

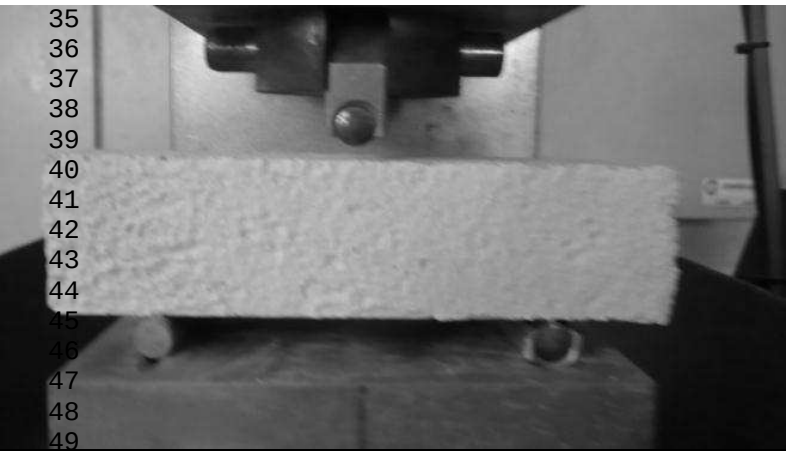

(a)

(b)

(c)

(d)

line figure
Click here to download line figure: fig6.eps

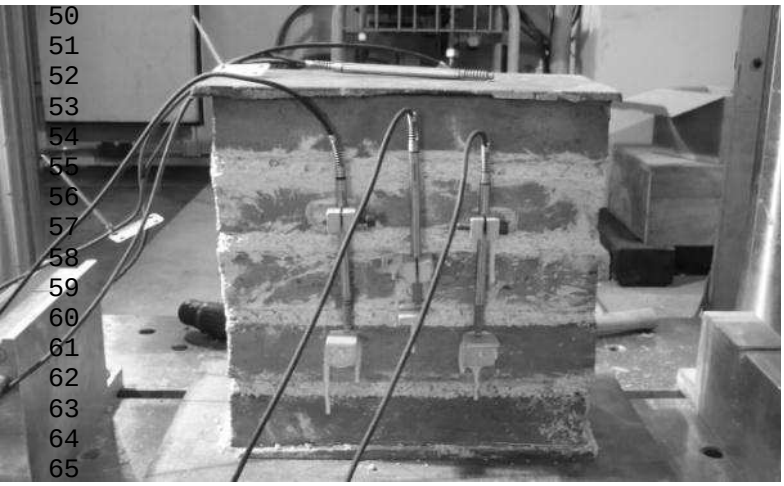

(a)

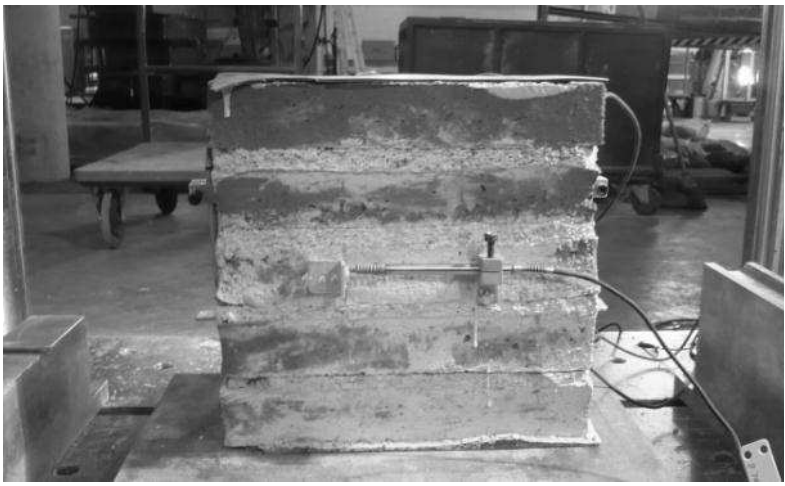

(b)

line figure
Click here to download line figure: fig7.eps

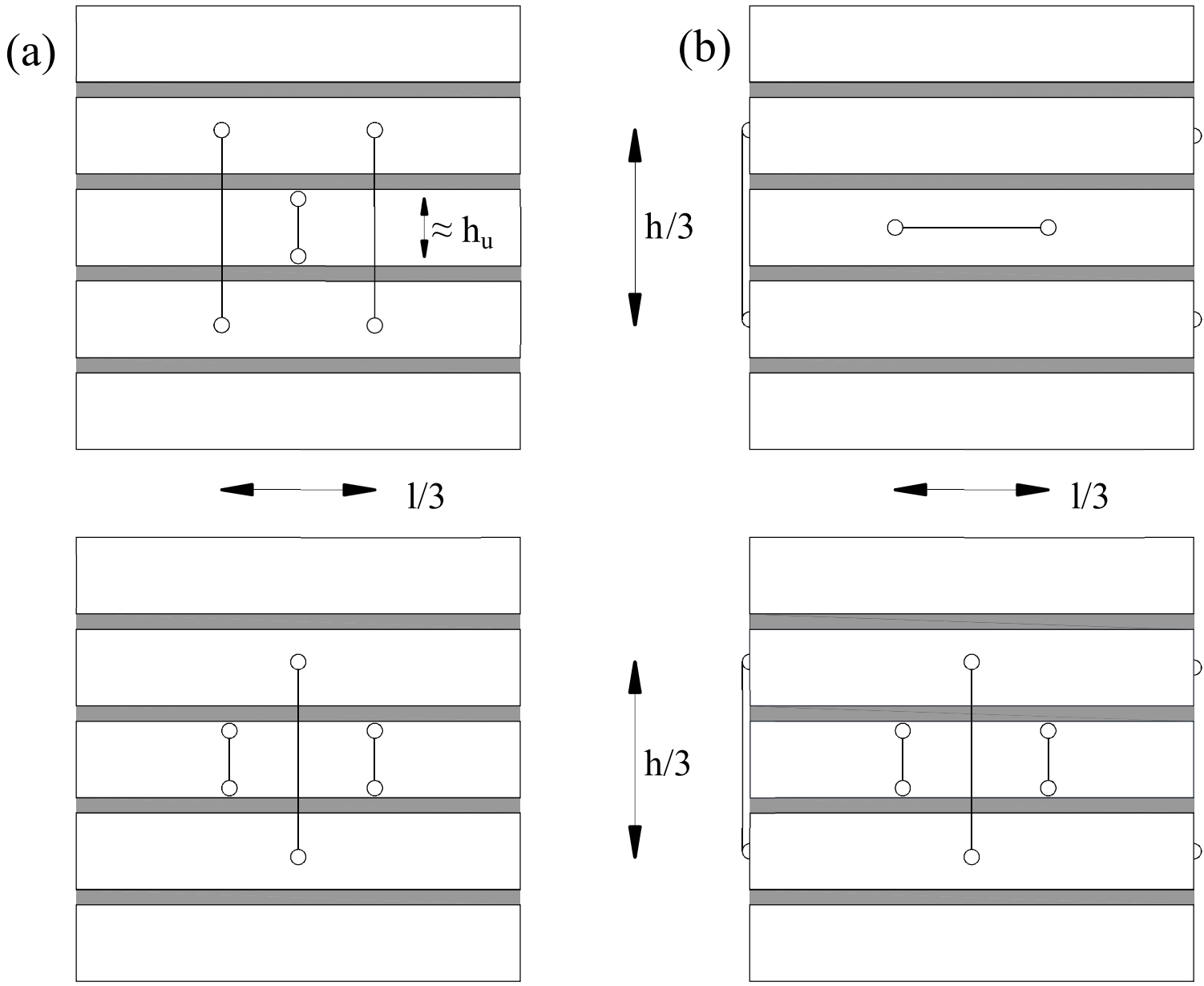

line figure
Click here to download line figure: fig8.eps

(a)

(b)

(c)

line figure
Click here to download line figure: fig9.eps

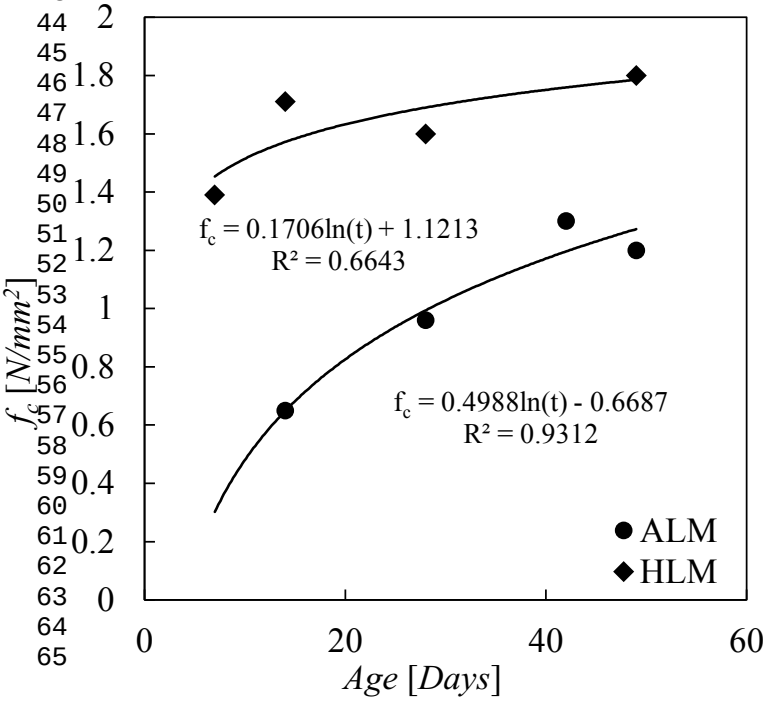

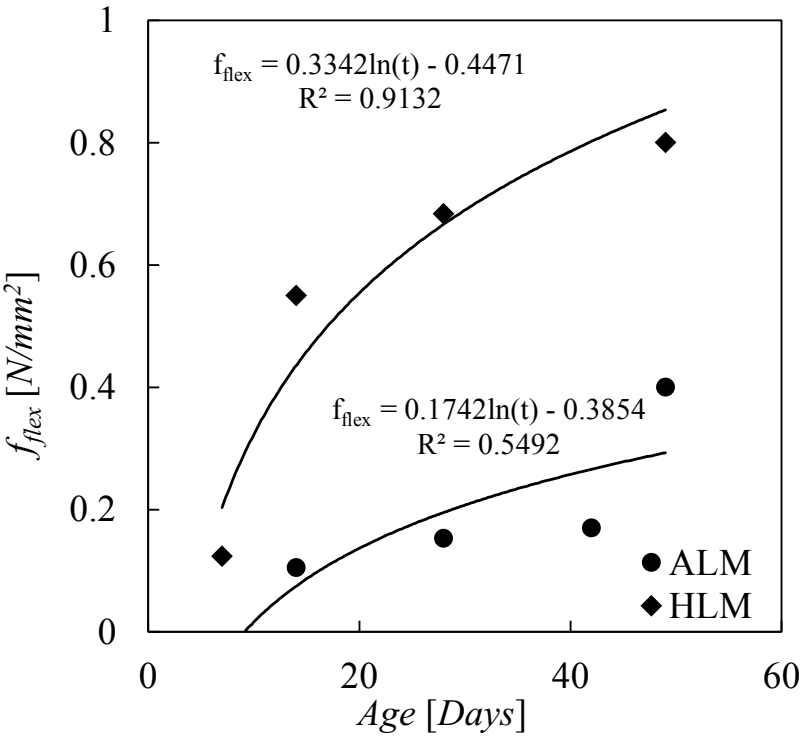

line figure

Click here to download line figure: fig10.eps

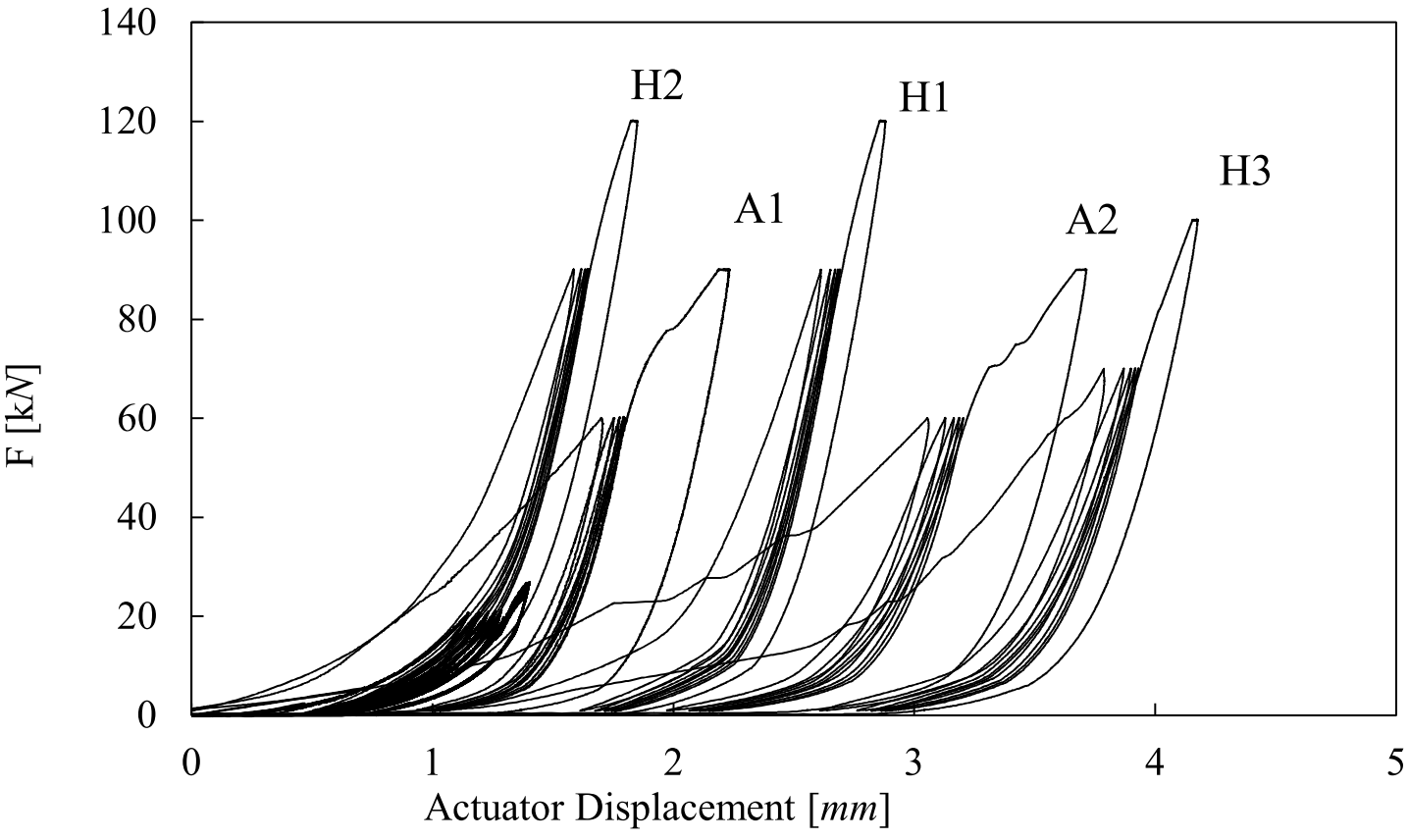

line figure

Click here to download line figure: fig11.eps

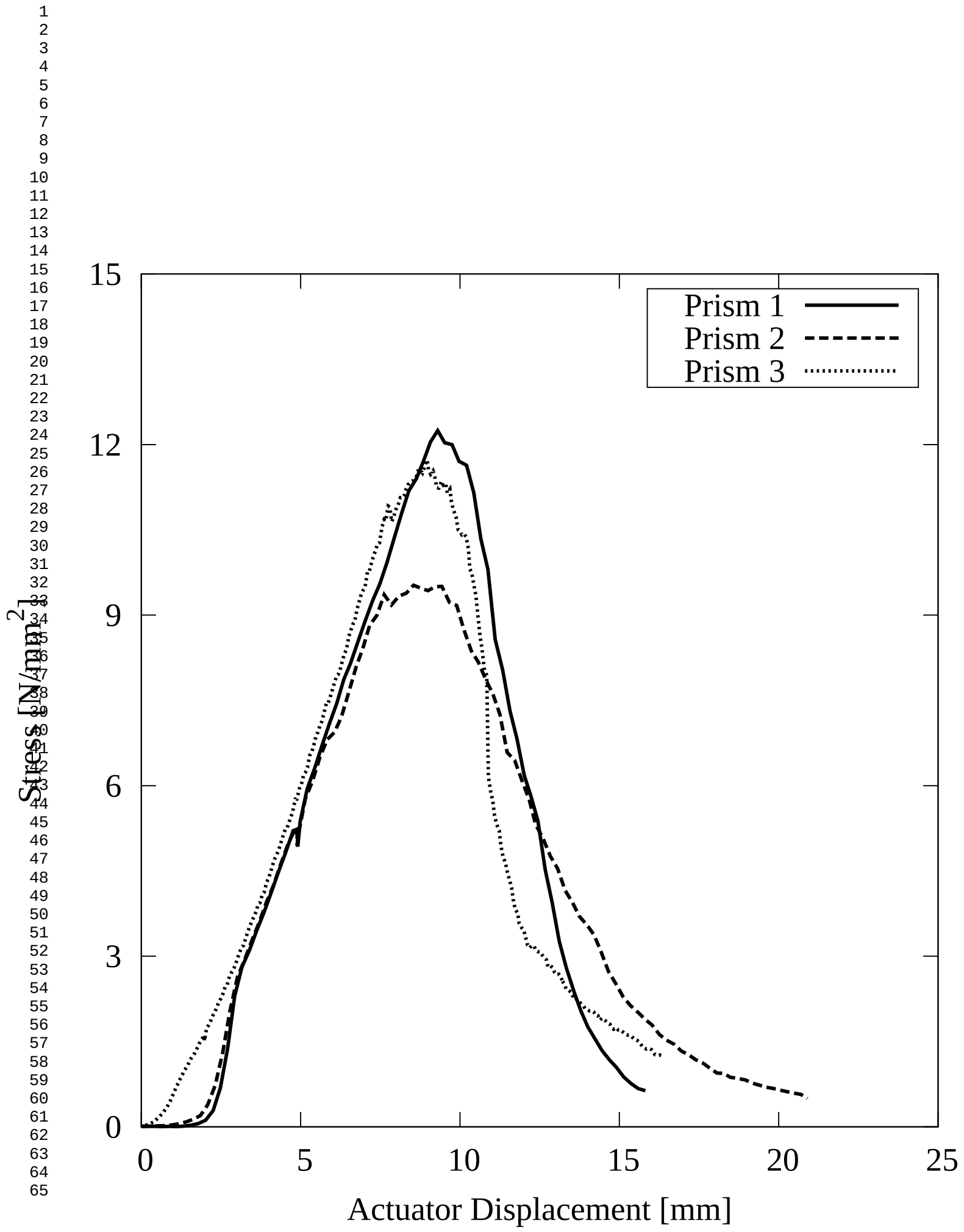

line figure
Click here to download line figure: fig12.eps

(a)

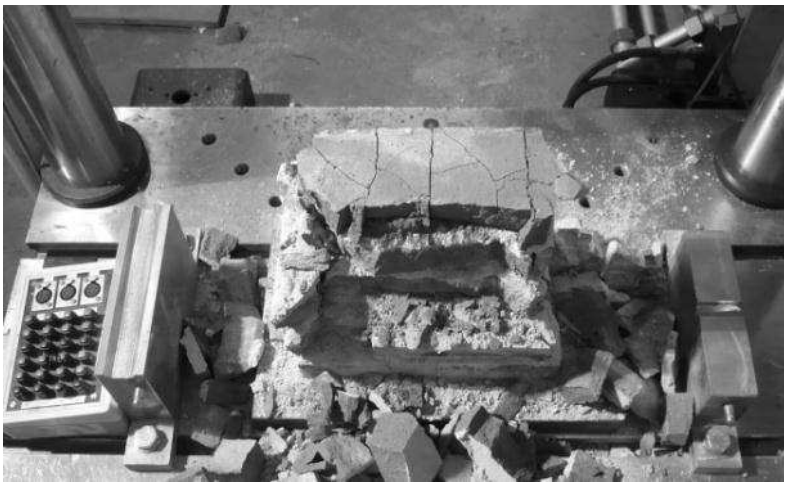

(b)

line figure
Click here to download line figure: fig13.eps

(a)

(b)

line figure

Click here to download line figure: fig14.eps

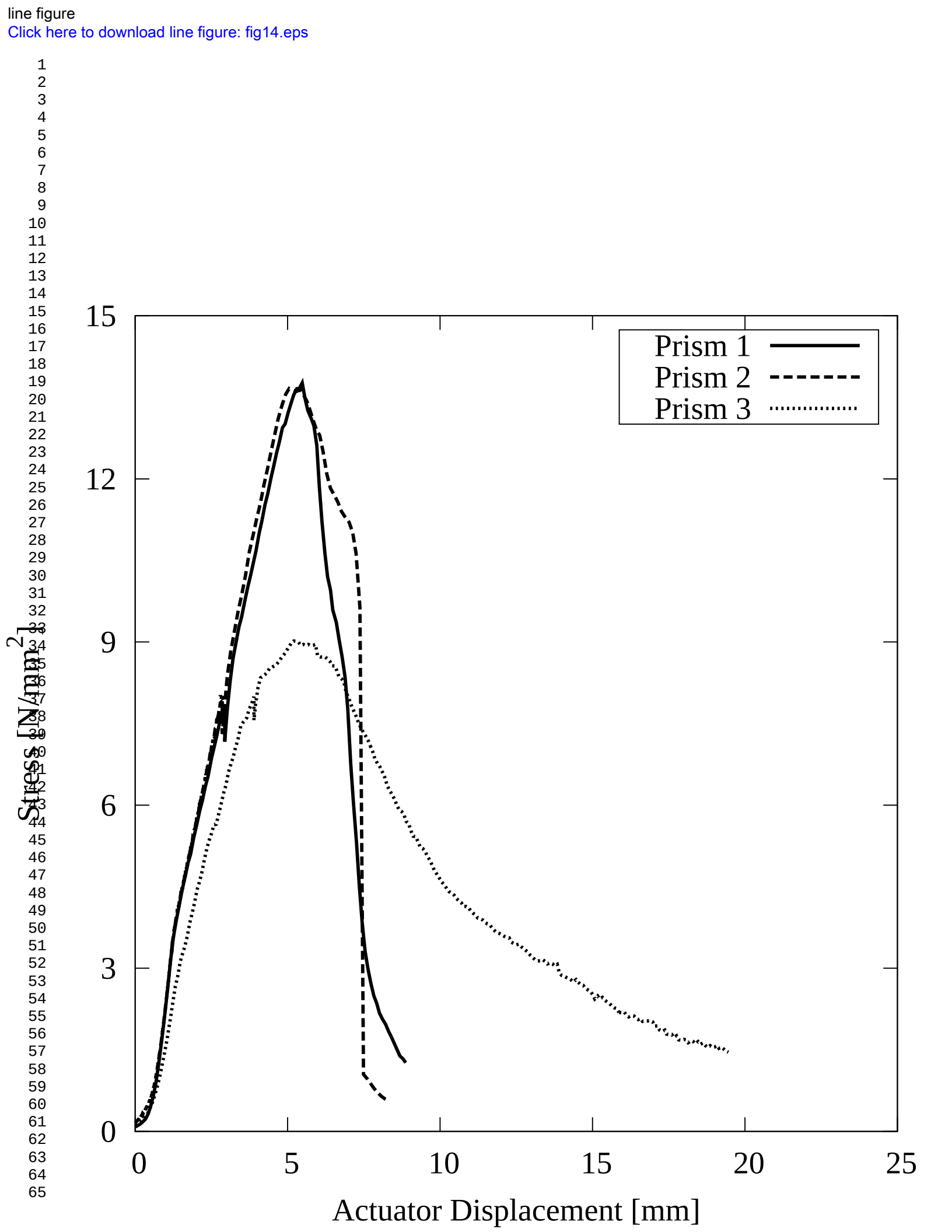

line figure
Click here to download line figure: fig15.eps

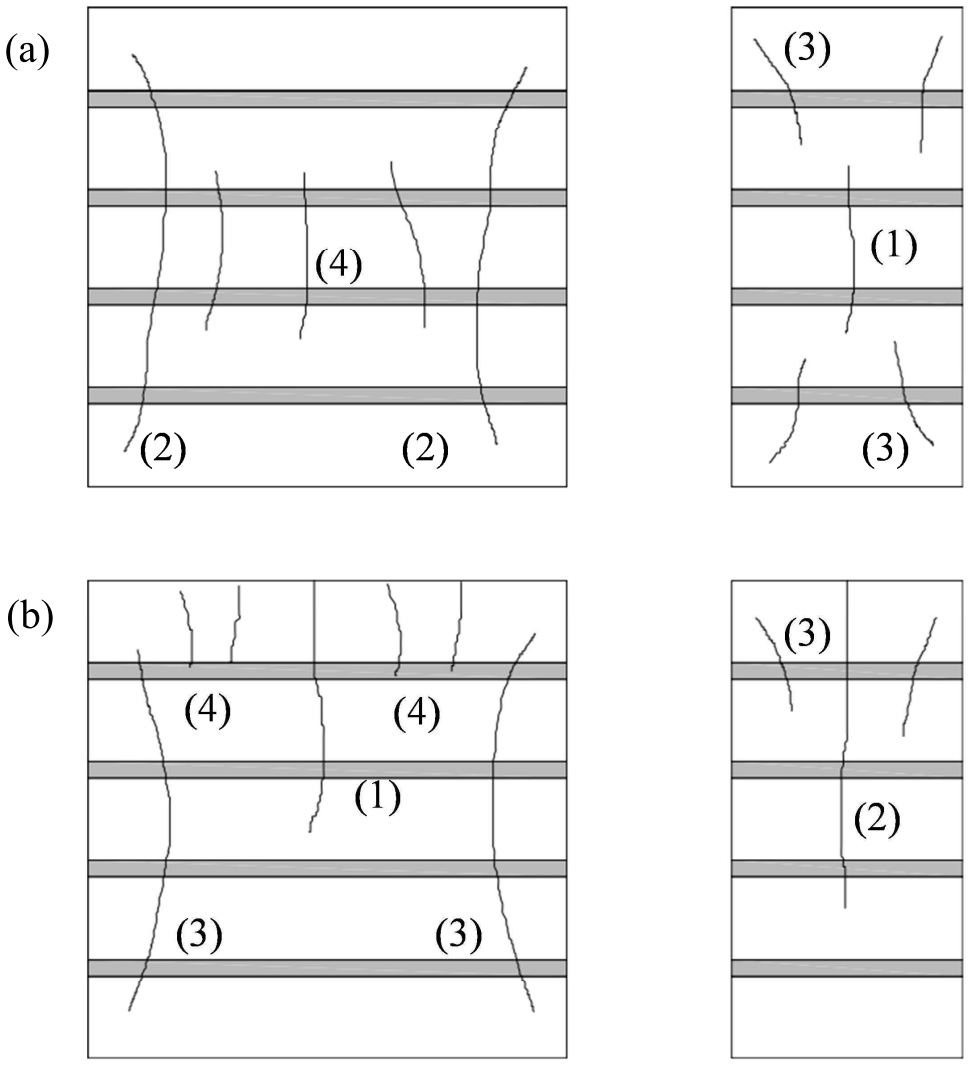

Table

Click here to download Table: Table1.docx

Sand Grain Size			
Sieve size [*mm*]	Weight % Retained	Cumulative Weight % Retained	Weight % Pass
5	0.2	0.2	99.8
4	1.13	1.33	98.67
2	18.86	20.19	79.81
1	30.21	50.4	49.6
0.5	18.24	68.65	31.35
0.25	11.43	80.08	19.92
0.125	7.28	87.36	12.64
0.063	6.87	94.23	5.77
Tray	4.29	98.52	1.48

Sand Properties	
Apparent density [kg/m^3]	1750
Particle density [kg/m^3]	2690
% saturated porosity	11.3
% Absorption	1.70

Table

Click here to download Table: Table2.docx

Sample	Height [mm]	Width [mm]	$f_{flex,u}$ [N/mm^2]	f_{tu} [N/mm^2]
I	39.25	135	7.71	3.39
II	42.00	134	7.06	3.18
III	42.25	134	7.11	3.21
Mean	41.17	134.33	7.29	3.26
St. Dev.	1.66	0.58	0.295	0.110
C.oV.	4.0%	0.4%	4.0%	3.4%

Table

Click here to download Table: Table3.docx

Single Samples	Height [mm]	f_{cu} [N/mm^2]	E_u [N/mm^2]	Double Samples	Height [mm]	f_{cu} [N/mm^2]	E_u [N/mm^2]	Triple Samples	Height [mm]	f_{cu} [N/mm^2]	E_u [N/mm^2]
I_1	39.5	28.5	3598	I_2+I_7	79	29.76	3795	IV_3+V_6+IV_1	125.25	22.02	5854
I_3	39.5	31.03	4054	II_2+II_7	85	21.87	4750	IV_4+IV_2+IV_5	124	16.57	5317
I_5	39.5	27.31	3872	II_1+II_4	84.75	23.38	4947	V_3+V_4+V_5	127	26.18	5068
I_6	39.5	22.56	2084	III_1+III_3	85.5	15.39	4389	VI_3+VI_7+VI_1	121.25	27.24	6038
II_3	42.25	21.86	3239	III_2+III_5	85.5	19.17	4801	VII_4+VII_6+VII_1	115	22.01	5394
II_6	42.25	24.41	4544	V_1+V_7	84.5	17.38	4863	VII_5+VII_2+VII_3	113.5	25.21	5730
III_4	42	22.69	2498	VI_2+VI_5	81.25	24.19	5057				
III_6	42.25	20.41	2181	VI_4+VI_6	81.25	19.22	4322				
IV_6	41.25	31.45	4488								
V_2	41.5	16.31	1304								
VII_7	38	26.54	5172								
Mean	40.68	24.83	3298	Mean	83.34	21.30	4653	Mean	121.00	23.21	5567
St. Dev.	1.51	4.64	1258	St. Dev.	2.48	4.53	493	St. Dev.	5.57	3.90	367
C.oV.	3.7%	18.7%	38.1%	C.oV.	3.0%	21.3%	10.6%	C.oV.	4.6%	16.8$	6.6%

Table

Click here to download Table: Table4.docx

Brick	I	II	III	IV	V	VI	VII	All
No. of tests	5	4	4	2	3	3	3	24
f_{cu} [N/mm^2]								
Mean	27.83	22.88	19.42	24.01	19.96	23.55	24.59	23.18
St. Dev.	3.261	1.244	3.056	10.519	5.418	4.047	2.328	2.86
C.oV.	11.7%	5.4%	15.7%	43.8%	27.1%	17.2%	9.5%	12.3%
E_u [N/mm^2]								
Mean	3481	3535	3467	4903	3745	5139	5432	4243
St. Dev.	798	1552	1319	586	2116	861	281	874
C.oV.	22.9%	43.9%	38.1%	12.0%	56.5%	16.7%	5.52%	20.6%

Table

Click here to download Table: Table5.docx

Sample	$f_{flex,m}$ [N/mm^2]	Sample	$f_{flex,m}$ [N/mm^2]
ALM1	0.23	HLM1	0.82
ALM2	0.55	HLM2	0.93
ALM3	0.18	HLM3	0.90
ALM4	0.20	HLM4	0.92
ALM5	0.71	HLM5	0.80
ALM6	0.72	HLM6	0.70
Mean	0.43	Mean	0.84
St. Dev.	0.235	St. Dev.	0.082
C.oV.	54.5%	C.oV.	9.6%

Table

Click here to download Table: Table6.docx

Sample	f_{cm} [N/mm^2]	Sample	f_{cm} [N/mm^2]
ALM1a	1.25	HLM1a	1.76
ALM1b	1.27	HLM1b	1.90
ALM2a	1.19	HLM2a	1.98
ALM2b	1.19	HLM2b	2.09
ALM3a	1.32	HLM3a	2.02
ALM3b	1.19	HLM3b	1.72
ALM4a	1.18	HLM4a	1.89
ALM4b	1.18	HLM4b	1.81
ALM5a	1.23	HLM5a	1.93
ALM15b	1.24	HLM5b	1.77
ALM6a	1.21	HLM6a	1.98
ALM6b	1.36	HLM6b	1.98
Mean	1.23	Mean	1.90
St. Dev.	0.061	St. Dev.	0.080
C.oV.	4.9%	C.oV.	4.2%

Table

Click here to download Table: Table7.docx

Sample	Height [*mm*]	f_c [N/mm^2]	Initial E_c [N/mm^2]	Unloading E_c [N/mm^2]	Final E_c [N/mm^2]
Prism 1	273	12.30	360	2574	488
Prism 2	266	9.68	474	2643	501
Prism 3	265	11.75	-	-	804
Mean	268	11.24	417	2609	598
St. Dev.	4.36	1.38	80.61	48.79	178.8
C.o.V.	1.6%	12.2%	19.3%	1.9%	29.9%
Mean (sulfur mortar caps)	-	12.03	-	-	-

Table

Click here to download Table: Table8.docx

Sample	Height [*mm*]	f_c [N/mm^2]	Initial E_c [N/mm^2]	Unloading E_c [N/mm^2]	Final E_c [N/mm^2]
Prism 1	265	13.80	1153	2836	1021
Prism 2	268	13.66	1326	2488	1053
Prism 3	280	9.05	1928	3078	1204
Mean	271	12.17	1469	2801	1093
St. Dev.	7.94	2.70	406.81	296.58	97.7
C.o.V.	2.9%	22.2%	27.7%	10.6%	8.9%
Mean (sulfur mortar caps)	-	13.73	-	-	-